Journal of Applied Mathematics and Computational Mechanics 2024, 23(4), 30-41
www.amcm.pcz.pl p-ISSN 2299-9965
DOI: 10.17512/jamcm.2024.4.03 e-ISSN 2353-0588

BUCKLING AND BENDING ANALYSIS OF POROUS FG BEAM USING A SIMPLE INTEGRAL QUASI-3D THEORY

Nabil Himeur[1], Abderrahmane Menasria[2,3], Abdelhakim Bouhadra[2,3], Mourad Chitour[1] Salah Refrafi[2], Loubna Guessoum[2], Aya Ouchene[2], Salima Lebouazda[2]

[1] Mechanical Engineering Department, Faculty of Sciences and Technology, University of Khenchela Khenchela, Algeria
[2] Civil Engineering Department, Faculty of Sciences and Technology, University of Khenchela Khenchela, Algeria
[3] Materials and Hydrology Laboratory, Civil Engineering Department, Faculty of Technology University of Sidi Bel Abbes, Sidi Bel Abbes, Algeria
himeur_nabil@univ-khenchela.dz, abderrahmane.menasria@univ-khenchela.dz
chitour.mourad@univ-khenchela.dz, refrafi_salah@univ-khenchela.dz
loubna.guessoum4@gmail.com, ayaouchene2023@gmail.com, lebouazdasalima1@gmail.com
abdelhakim.bouhadra@univ-khenchela.dz

Received: 2 May 2024; Accepted: 30 October 2024

Abstract. This paper introduces a simplified approach to analyze the buckling and static bending of advanced composite beams, including functionally graded materials (FGMs), with various porosity distributions. This method uses a simple integral quasi-3D approach with a higher-order shear deformation theory, which offers several advantages: reduced complexity by requiring fewer unknowns and governing equations compared to other methods; improved accuracy by incorporating the effect of stretching across the beam's thickness, leading to more accurate results; finally, accurate shear representation by satisfying the zero-traction boundary conditions on the beam's surfaces without needing a shear correction factor; and it captures the parabolic distribution of the transverse shear strain and stress across the thickness. The virtual work principle is used to derive the governing equations, and the Navier solution is employed to find analytical solutions for buckling and static bending of various boundary conditions for FGM porous beams. The proposed method agrees well with the literature on FGMs and other advanced composite beams. Finally, numerical results showcase how material distribution (including power-law FGMs), geometry, and porosity affect the beam's deflections, stresses, and critical buckling load.

MSC 2010: *74B05, 74E05, 74S25*
Keywords: *higher-order shear deformation theory, FG beam, integral quasi-3D, bending, buckling, porosity, virtual work principle, Navier solution*

1. Introduction

Functionally graded materials (FGMs) are novel engineered materials with properties continuously varying throughout their structure. This gradual change in composition and microstructure distinguishes them from conventional composite materials, which typically have distinct layers with abrupt property changes. FGMs can be designed to meet the specific requirements of diverse applications, from high-temperature components in aerospace engineering to wear-resistant surfaces in tribological applications [1].

The unique properties of functionally graded materials (FGMs) have attracted significant research interest in their bending behavior under various loading conditions. This includes static bending, free vibration analysis, and buckling behavior of FGM beams, plates, and shells [2, 3]. Literature suggests that FGM plate analysis can be approached through various theoretical frameworks, including classical plate theory (CPT) [4], first-order shear deformation theory (FSDT) [5, 6], and higher-order shear deformation theory (HSDT) [7, 8].

According to the literature, certain research using a higher shear deformation plate theory HSDT using integral terms to determine the behaviour of plates in FGM has been published. In [9], the authors proposed a new and simple Higher-Order Shear Deformation Theory (HSDT) to analyze the thermal stability of functionally graded (FG) sandwich plates, this analysis aims to determine the critical temperature at which the FG sandwich plate buckles due to thermal loads. Messaoudi et al. [10] used a simplified approach to the problem by utilizing a new displacement field with fewer unknowns than existing quasi-3D shear deformation theories. Chitour et al. [11] proposed a theoretical framework for deriving the equilibrium equations governing the behavior of functionally graded (FG) sandwich beams. This framework allowed them to obtain analytical solutions for bending problems in these beams. Several research works on FGM beams using different types of materials, loading, and boundary conditions have recently been published [12-16].

Various publications have explored the effect of porosity on the behavior of FGM beams, Ghazwani et al. [17] studied the nonlinear forced vibrations of sandwich beams made from porous functionally graded materials (FGMs) with a viscoelastic core layer. Their analysis employs higher-order Zig-Zag theories for normal and shear deformations within the viscoelastic core. The study examines how these beams vibrate under external forces, considering the FGM faces' porosity and the core layer's viscoelastic nature. The higher-order Zig-Zag theory incorporates the effects of both bending and shear deformations within the core material [18-20].

This work aims to develop an original 2D and quasi-3D HSDT shear deformation theory, including integral terms, to study the static bending and buckling behavior of FG beams having porosities. The proposed beam has four types of porous distribution and is investigated under static bending and buckling with varied boundary conditions. To analyze the beam's behavior, the governing equations are derived using the principle of virtual work and then solved using the Navier technique. To validate the accuracy and effectiveness of this new theory, the calculated results are compared with those obtained from other established theories. Additionally, the paper presents and discusses a comprehensive set of parametric studies to explore the influence of various parameters on the system's behavior.

2. Imperfect FGM beams material properties

The FG beam varied boundary conditions of length (l), thickness (h), and width (b) is exposed where the material properties of a P-FGM composition vary along z direction with the FG index k (Fig. 1):

$$P(z) = P_m + (P_c - P_m)V(z) \quad \text{and} \quad V(z) = \left(\frac{1}{2} + \frac{z}{h}\right)^k \tag{1}$$

$P(z)$ is the variation in mechanical properties across the thickness, and $V(z)$ is the volume fraction of the ceramic.

Four porosity models are used (Fig. 1b), [18].

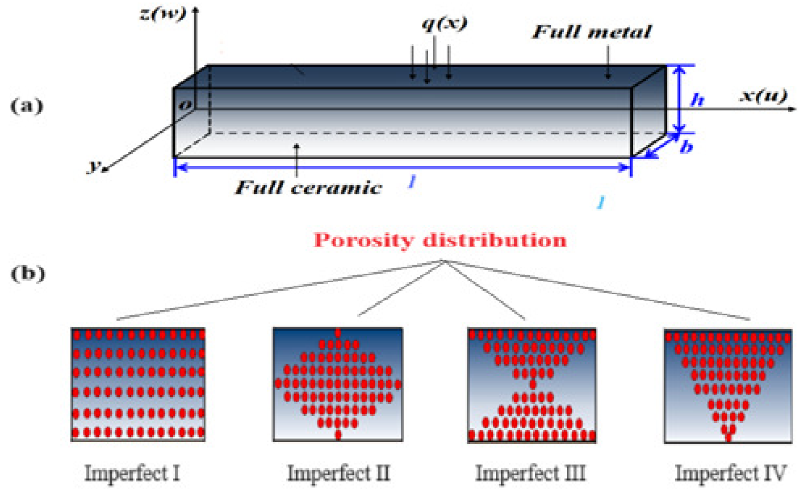

Fig. 1. Geometry and coordinate system of the imperfect FG beam

Porous material properties for various porosity patterns and porosity coefficient (Ω) are given by:

$$\begin{aligned}
&\textit{Imperfect I } (\text{H-Pattern}): P(z) = (P_c - P_m)V_c + P_m - \frac{\Omega}{2}(P_c + P_m) \\
&\textit{Imperfect II } (\text{O-Pattern}): P(z) = (P_c - P_m)V_c + P_m - \frac{\Omega}{2}(P_c + P_m)\left(1 - \frac{2|z|}{h}\right) \\
&\textit{Imperfect III } (\text{X-Pattern}): P(z) = (P_c - P_m)V_c + P_m - \frac{\Omega}{2}(P_c + P_m)\left(\frac{1}{2} + \frac{z}{h}\right) \\
&\textit{Imperfect III } (\text{V-Pattern}): P(z) = (P_c - P_m)V_c + P_m - \frac{\Omega}{2}(P_c + P_m)\left(\frac{2|z|}{h}\right)
\end{aligned} \tag{2}$$

3. Theoretical formulations of the FG beam

3.1. Kinematics and strains

The displacement field of the conventional HSDT is given by:

$$\begin{aligned} u(x,z) &= u_0(x) - z\frac{\partial w_0}{\partial x} + k_a\, f(z)\int \theta(x)\,dx \\ w(x,z) &= w_0(x) + n\, g(z)\theta(x) \end{aligned} \tag{3}$$

where u_0, w_0, θ are the three unknown displacements of the mid-plane of the beam. By a Navier-type method, the integrals used in the above equations can be given:

$$\int \theta\, dx = A'\frac{\partial \theta}{\partial x},\ A' = -\frac{1}{\alpha^2},\ k_a = -\alpha^2 \ \text{ and } \ \alpha = \frac{m\pi}{l} \tag{4}$$

Where the coefficient A' is expressed according to the type of solution used, in this case via Navier.

$f(z)$ represents the shape function is represented as:

$$f(z) = z\left(1 - \frac{4}{3}\frac{z^2}{h^2}\right) \ \text{ and } \ g(z) = \frac{2}{15}\frac{df(z)}{dz} \tag{5}$$

n is a real number given as $n = 0$ for 2D and $n = 1$ for quasi-3D.

The non-zero linear strain components obtained from Eqs. (3) and (4) are:

$$\varepsilon_x = \varepsilon_x^0 + zk_x^b + f(z)k_x^s,\ \left\{\gamma_{xz}\right\} = f'(z)\left\{\gamma_{xz}^0\right\} + g(z)\left\{\gamma_{xz}^1\right\},\ \varepsilon_z = g'(z)\,\varepsilon_z^0 \tag{6a}$$

$$\left\{\varepsilon_x^0\right\} = \left\{\frac{\partial u_0}{\partial x}\right\},\ \begin{Bmatrix} k_x^b \\ k_x^s \end{Bmatrix} = \begin{Bmatrix} -\dfrac{\partial^2 w_0}{\partial x^2} \\ k_1\theta \end{Bmatrix},\ \left\{\gamma_{xz}^0\right\} = \left\{k_1\int \theta\, dx\right\},\ \left\{\gamma_{xz}^1\right\} = \left\{\frac{\partial \theta}{\partial x}\right\},\ \varepsilon_z^0 = \theta \tag{6b}$$

The linear elastic constitutive equations at a point are:

$$\begin{Bmatrix} \sigma_x \\ \sigma_z \\ \tau_{xz} \end{Bmatrix} = \begin{bmatrix} C_{11} & C_{13} & 0 \\ C_{13} & C_{33} & 0 \\ 0 & 0 & C_{55} \end{bmatrix} \begin{Bmatrix} \varepsilon_x \\ \varepsilon_z \\ \gamma_{xz} \end{Bmatrix} \tag{7}$$

The C_{ij} $(i, j = 1, 3, 5)$ expressions in terms of engineering constants:

- Case of 2D $(\varepsilon_z = 0)$, then C_{ij} are:

$$C_{ij} = E,\ (i=1);\ C_{ii} = \frac{E(z)}{2\left(1+\nu(z)\right)},\ (i=5) \tag{8a}$$

- Case of Quasi-3D $(\varepsilon_z \neq 0)$, then C_{ij} are:

$$C_{ii} = \frac{E(z)}{1-\nu^2(z)},\ (i=1,3);\ \ C_{ij} = \frac{E(z)\nu(z)}{1-\nu^2(z)},\ (i,j=1,3);\ \ C_{ii} = \frac{E(z)}{2\left(1+\nu(z)\right)},\ (i=5) \quad \text{(8b)}$$

3.2. Governing equations

Using the principle of virtual work can be expressed as

$$\begin{aligned}\delta U - \delta V = &\left(\int_A \left[N_x \delta\varepsilon_x^0 + N_z \delta\varepsilon_z^0 + M_x^b \delta k_x^b + M_x^s \delta k_x^s + Q_{xz} \delta\gamma_{xz}^0 + S_{xz} \delta\gamma_{xz}^1 \right] dA \right) \\ &- \left(\int_A q\delta w_0\, dA - \int_A qg(z)\delta\theta\, dA - \int_A N_0 \frac{d(w_0 + g(z)\theta(x))}{dx} \frac{d\delta(w_0 + g(z)\theta(x))}{dx} dA \right) = 0\end{aligned} \quad (9)$$

Where A is the surface, and stress resultants N, M, Q and S are the force and moment components represented in the following forms

$$\begin{Bmatrix} N_x \\ M_x^b \\ M_x^s \end{Bmatrix} = \int_{-h/2}^{h/2} (\sigma_x) \begin{Bmatrix} 1 \\ z \\ f(z) \end{Bmatrix} dz,\ \ N_z = \int_{-h/2}^{h/2} \sigma_z\, g'(z)\, dz,\ \ \begin{Bmatrix} S_{xz} \\ Q_{xz}^s \end{Bmatrix} = \int_{-h/2}^{h/2} (\tau_{xz}) \begin{Bmatrix} g(z) \\ f'(z) \end{Bmatrix} dz \quad (10)$$

From Eq. (6) into Eq. (9), the following governing equations are obtained:

$$\begin{aligned} &\delta u_0: \quad \frac{\partial N_x}{\partial x} = 0 \\ &\delta w_0: \quad \frac{\partial^2 M_x^b}{\partial x^2} + q + N_0 \frac{\partial^2 w}{\partial x^2} = 0 \\ &\delta\theta: \quad -\mathrm{N}_z - k_1 M_x^s + k_1 A' \frac{\partial Q_{xz}}{\partial x} + \frac{\partial S_{xz}}{\partial x} + qg(z) + N_0 g(z)^2 \frac{\partial^2 w}{\partial x^2} = 0 \end{aligned} \quad (11)$$

Using Eqs. (6), (7) and (8b), the stress resultants are obtained as:

$$\begin{Bmatrix} N \\ M_x^b \\ M_x^s \end{Bmatrix} = \begin{bmatrix} A & B & B^s \\ B & D & D^s \\ B^s & D^s & H^s \end{bmatrix} \begin{Bmatrix} \varepsilon_x^0 \\ k_x^b \\ k_x^s \end{Bmatrix} + \begin{bmatrix} L \\ L^a \\ R \end{bmatrix} \varepsilon_0^z \quad \text{(12a)}$$

$$\begin{Bmatrix} Q \\ S \end{Bmatrix} = \begin{bmatrix} F^s & X^s \\ X^s & A^s \end{bmatrix} \begin{Bmatrix} \gamma^0 \\ \gamma^1 \end{Bmatrix},\ \ N_z = R^a \varepsilon_z^0 + L\left(\varepsilon_x^0\right) + L^a\left(k_x^b\right) + R\left(k_x^s\right) \quad \text{(12b)}$$

$$\left\{A \quad B \quad D \quad B^s \quad D^s \quad H^s\right\} = \int_{-h/2}^{h/2} \lambda(z)\left[1, z, z^2, f(z), zf(z), f^2(z)\right] \begin{Bmatrix} \dfrac{1-\nu}{\nu} \\ 1 \\ \dfrac{1-2\nu}{2\nu} \end{Bmatrix} dz \quad (13a)$$

$$S = \{S_{xz}\},\ Q = \{Q_{xz}\},\quad \begin{Bmatrix} L \\ L^a \\ R \\ R^a \end{Bmatrix} = \int_{-h/2}^{h/2} \lambda(z) \begin{Bmatrix} 1 \\ z \\ f(z) \\ g'(z)\dfrac{1-\nu}{\nu} \end{Bmatrix} g'(z)\, dz \quad (13b)$$

$$\left(F_{44}^s, X_{44}^s, A_{44}^s\right) = \int_{-h/2}^{h/2} \left(\frac{E(z)}{2(1+\nu)} \left[f'^2(z), f'(z)g(z), g^2(z) \right] \right) dz$$
$$F^s = F_{44}^s,\ A^s = A_{44}^s,\ X^s = X_{44}^s \quad (13c)$$

Substituting Eqs. (6), (12), (13) into Eq. (11), the stability equations are defined by:

$$\delta u_0 : A\frac{\partial^2 u_0}{\partial x^2} - B\frac{\partial^3 w_0}{\partial x^3} + \left(B^s k_1 + L\right)\frac{\partial \theta}{\partial x} = 0$$
$$\delta w_0 : B\frac{\partial^3 u_0}{\partial x^3} - D\frac{\partial^4 w_0}{\partial x^4} + \left(D_{11}^s k_1 + L^a\right)\frac{\partial^2 \theta}{\partial x^2} + q + N_0\frac{\partial^2 w}{\partial x^2} = 0$$
$$\delta\theta : -\left(L + k_1 B_{11}^s\right)\frac{\partial u_0}{\partial x} + \left(L^a + k_1 D_{11}^s\right)\frac{\partial^2 w_0}{\partial x^2} - \left(k_1{}^2 H_{11}^s + 2k_1 R + R^a\right)\theta +$$
$$\left(k_1^2 A'^2 F_{44}^s + k_1 A' X_{44}^s\right)\frac{\partial^2 \theta}{\partial x^2} + \left(A_{44}^s + k_1 A' X_{44}^s\right)\frac{\partial^2 \theta}{\partial x^2} + qg(z) + N_0 g(z)^2\frac{\partial^2 w}{\partial x^2} = 0 \quad (14)$$

3.3. Exact solution for various boundary conditions of FG beam

The exact solution of Eqs. (14) for the FGM beams under various boundary conditions can be constructed by using the admissible functions listed in Table 1.

Table 1. Admissible functions *Xm*, *Yn*

Boundary conditions	Admissible functions *Xm* and *Yn*	
	Xm	*Yn*
SS	$\sin(\alpha x)$	$\sin(\lambda x)$
CC	$\sin(\alpha x)\cos(\alpha x)$	$\sin(\lambda x)\sin(\lambda x)$
CF	$\cos^2(\alpha x)(\sin^2(\alpha x)+1)$	$\sin^2(\lambda x)$

With $\alpha = m\pi/l$ and $\lambda = n\pi/b$

$$\begin{Bmatrix} u_0(x,y) \\ w_0(x,y) \\ \theta(x,y) \end{Bmatrix} = \begin{Bmatrix} U_m \dfrac{\partial X_m(x)}{\partial x} Y_n(x) \\ W_m \quad X_m(x) Y_n(x) \\ \theta_m \quad X_m(x) Y_n(x) \end{Bmatrix} \tag{15}$$

where U_m, W_m and θ_m are the unknown displacement coefficients.

By replacing the extensions of U_m, W_m and θ_m of equations (14) in the equations of equilibrium (12), the analytical solutions can be obtained from

$$\begin{bmatrix} a_{11} & a_{12} & a_{13} \\ a_{12} & a_{22}+N_{cr} & a_{23} \\ a_{13} & a_{23} & a_{33} \end{bmatrix} \begin{Bmatrix} U_{mn} \\ W_{mn} \\ \theta_{mn} \end{Bmatrix} = \begin{Bmatrix} 0 \\ 0 \\ 0 \end{Bmatrix} \tag{16}$$

$$\begin{aligned} &a_{11} = A_{11}L_{12},\ \ a_{21} = -BL_{13},\ \ a_{12} = -BL_{12},\ \ a_{22} = DL_{13},\ \ a_{13} = B^s k_1 L_{12} - LL_{12} \\ &a_{31} = B^s k_1 L_{13} - LL_{13},\ \ a_{23} = -D^s k_1 L_{13} + L_a L_{13},\ \ a_{32} = -D^s k_1 L_{13} + L_a L_{13} \\ &a_{33} = H_{11}^s k_1^2 L_9 - 2k_1 R L_{13} + R - A^2 F_{44}^s k_1^2 L_{13} - 2AX_{44}^s k L_{13} - A_{44}^s L_{13},\ \ N_{cr} = N_0 L_9 \end{aligned} \tag{17}$$

The transverse load $q(x)$ is also expanded in a Fourier series as

$$q = \sum_{m=1}^{\infty} q_m \sin\frac{m\pi x}{l} \tag{18}$$

The Fourier coefficient (q_m) for sinusoidal and uniform loads are as follows

$$q = \begin{cases} q_0 & \text{Sinusoidal load} \quad (m=1) \\ \dfrac{4q_0}{m\pi} & \text{Uniform load} \quad (m = 1, 3, 5 \ldots \infty) \end{cases} \tag{19}$$

For the bending problem, put $N_0 = 0$; for the buckling problem, put $q = 0$.

- Bending analysis

$$[K]\{\Delta\} = \{f\} \tag{20}$$

- Buckling analysis

$$\{[K] - N_0[N]\}\{\Delta\} = \{0\} \tag{21}$$

Where $[K]$ is the stiffness matrix, $[N]$ is the geometric matrix due to the axial forces, $\{f\}$ is the force vector, $\{\Delta\}$ is the vector of unknowns, and N_0 is the axial force.

4. Numerical results and discussion

4.1. Convergence and validation study

In this paper, the properties of the materials used are: for ceramic (P_c: Alumina, Al_2O_3): E_c = 380 GPa; υ_c = 0.3, for metal (P_m: Aluminum, Al): E_m = 70 GPa; υ_m = 0.3. For simplicity, displacements, stresses and critical buckling loads are presented in non-dimensional form:

$$\begin{gathered}\bar{w}=\frac{100E_m h^3}{q_0 l^4}w\left(x=\frac{l}{2},z=0\right),\ \ \bar{u}=\frac{100E_m h^3}{q_0 l^4}u\left(x=0,z=-\frac{h}{2}\right),\\ \bar{\sigma}_{xx}(z)=\frac{h}{q_0 l}\sigma_x\left(x=\frac{l}{2},z=\frac{h}{2}\right),\ \ \bar{\tau}_{xz}(z)=\frac{h}{q_0 l}\tau_{xz}\left(x=0,z=0\right),\ \ Ncr=N_0\frac{12l^2}{E_m h^3}\end{gathered}\tag{22}$$

Table 2 presents the maximum nondimensionalized displacements and stresses of the beam for various power law index values and a length-to-thickness (L/h) ratio equal to 5. To facilitate comparison, we generated numerical results for a supported functionally graded (FG) beam using different theories. It is observed from Table 2 that the transverse displacement reaches its maximum value when $k = \infty$, while it is minimized when $k = 0$. This behavior is attributed to the increased flexibility of FG beams with higher power law indices.

Table 2. Non-dimensional displacements and stresses of functionally graded beams (L = 5h)

k	Theory	Model	Uniform load			
			$\bar{u}$	$\bar{w}$	$\bar{\sigma}_x$	$\bar{\tau}_{zx}$
0 ceramic	Present 2D	HSDT	0.9398	3.1653	3.8020	0.7333
	Present 3D	HSDT	0.9080	2.8951	3.4120	0.6599
	Sayyad & Ghugal [20]	RSDT	0.9420	3.1635	3.8084	0.7764
	Reddy [21]	HSDT	0.9397	3.1654	3.8028	0.7305
	Timoshenko [22]	FSDT	0.9210	3.1057	3.7501	0.4922
	Bernoulli-Euler [23]	CBT	0.9210	2.8783	3.7501	–
5	Present 2D	HSDT	3.7101	9.8280	8.1100	0.7398
	Present 3D	HSDT	3,4893	8,6286	7,1326	0.7000
	Sayyad & Ghugal [20]	RSDT	3.7179	9.8414	8.1331	0.7654
	Reddy [21]	HSDT	3.7098	9.8281	8.1127	0.8114
	Timoshenko [22]	FSDT	3.6496	9.4987	7.9430	1.5373
	Bernoulli-Euler [23]	CBT	3.6496	8.7508	7.9430	–
10	Present 2D	HSDT	3.8861	10.938	9.7128	0.6715
	Present 3D	HSDT	3.6709	9.5508	8.5406	0.6353
	Sayyad & Ghugal [20]	RSDT	3.9858	10.94	9.7345	0.6947
	Reddy [21]	HSDT	3.8861	10.938	9.7141	0.6448
	Timoshenko [22]	FSDT	3.8096	10.534	9.5231	1.9050
	Bernoulli-Euler [23]	CBT	3.8096	9.6072	9.5231	–
∞ metal	Present 2D	HSDT	5.1018	17.183	3.8020	0.7482
	Present 3D	HSDT	4,9290	15.716	3.4120	0.7079
	Sayyad & Ghugal [20]	RSDT	5.1133	17.173	3.8084	0.7741
	Reddy [21]	HSDT	5.1021	17.183	3.8028	0.7305
	Timoshenko [22]	FSDT	5.0000	15.912	3.7501	0.4922
	Bernoulli-Euler [23]	CBT	5.0000	15.625	3.7501	–

The analysis of Table 3 indicates that the findings from this theory align closely with those from other theories. The clamped (C-C) beams demonstrate the highest buckling loads, unlike the cantilever (C-F) beams, which show the lowest. Additionally, an increase in the power law index is associated with a decrease in normalized buckling loads, confirming the current theory's capability to accurately determine the critical buckling loads of P-FGM beams under varying boundary conditions.

Table 3. Comparison of the normalized buckling loads of functionally graded beams with different boundary conditions ($L/h = 5$)

BC's	Theory	k					
		0	1	2	5	10	∞
	Present 2D	48.5957	24.5837	19.0709	15.6436	14.0512	8.95187
SS	Present 3D	49.6392	25.372	19.8365	16.4111	14.6969	9.14408
	Sayyad & Ghugal [20]	48.626	24.5966	19.0738	16.622	14.0485	8.95730
	Kahya & Turan [24]	48.5907	24.5815	19.1617	15.9417	14.3445	8.95100
	Nguyen et al. [25]	48.8406	24.6894	19.1577	15.7355	14.1448	–
CC	Present 2D	152.148	79.4832	60.8785	46.8871	40.9883	28.0272
	Present 3D	171.629	89.382	69.6172	55.9988	49.4489	31.6159
	Sayyad & Ghugal [20]	154.484	79.739	61.9488	49.5646	42.7493	27.9160
	Kahya & Turan [24]	151.943	79.3903	61.7449	49.5828	43.5014	27.9890
	Nguyen et al. [25]	154.561	80.5940	61.7666	47.7174	41.7885	–
CF	Present 2D	13.0542	6.5362	5.0958	4.2906	3.8527	2.3807
	Present 3D	14.2703	6.8319	5.2547	4.4028	3.9351	2.3945
	Sayyad & Ghugal [20]	13.0719	6.557	5.0986	4.2931	3.8512	2.3819
	Kahya & Turan [24]	13.0594	6.5352	5.0981	4.2926	3.897	2.4057
	Nguyen et al. [25]	13.0771	6.5427	5.0977	4.2772	3.882	–

4.2. Parametric study and discussions – porosity effect

Figure 2 indicates the effect of the side-to-thickness ratio l/h and the porosity models on the central deflections w of FG porous beams with volume fraction $k = 2$, and porosity coefficient Ω is chosen as 0.2. The central deflections (w) decrease with an increasing in side-to-thickness ratio for the various porous models.

Variation of the transverse shear stress τ_{xz} and the axial stress σ_{xx} through-the-thickness FG beams for various porous models with volume fraction $k = 2$ and the side-to-thickness ratio $l/h = 10$ are shown in Figure 3. Figure 3b predicts a parabolic distribution of transverse shear stress throughout the depth of FG porous beams. Overall, it is noted that the present results show excellent agreement with higher-order theories. In addition, the magnitude of the tensile stresses given in Figure 3a is greater than the magnitude of the compressive stresses in FG porous beams.

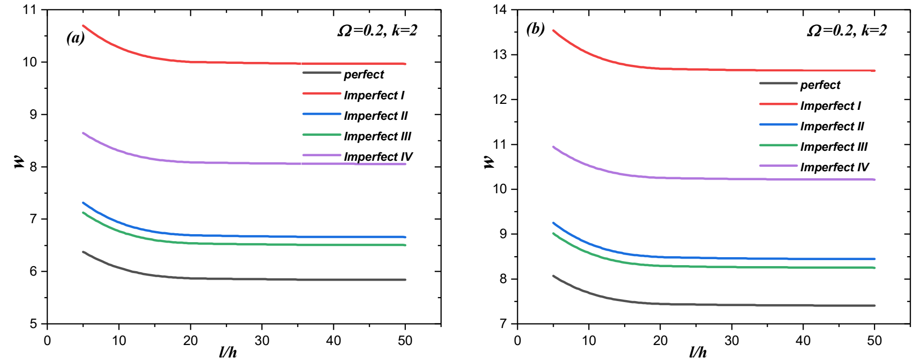

Fig. 2. Variation of the non-dimensional central deflection w versus l/h of perfect and imperfect beams ($k = 2$): a) sinusoidally distributed loads, b) uniform distributed loads

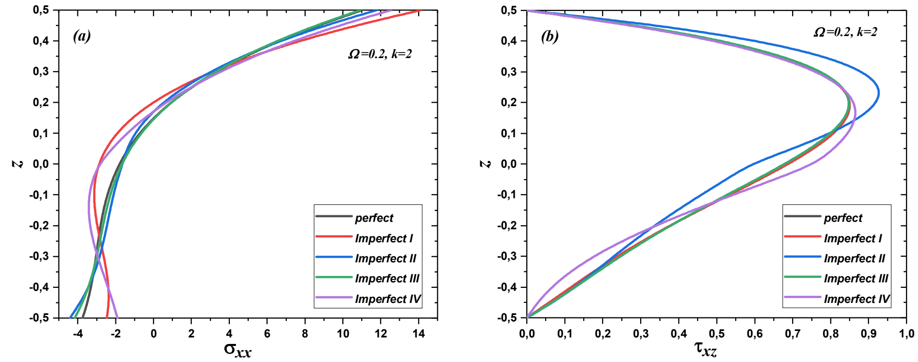

Fig. 3. The variation of stress through-the-thickness of perfect and imperfect beams l/h =10 ($k = 2$) under uniform distributed loads: a) axial stress σxx, b) transverse stress τxz

Figure 4 shows the variation of the non-dimensional critical buckling load of both boundary conditions supported (*SS*) and clamped (*CC*) FG porous beams concerning L/h ratios. The critical buckling load N_{cr} is almost constant after $L/h = 20$ for all porous models.

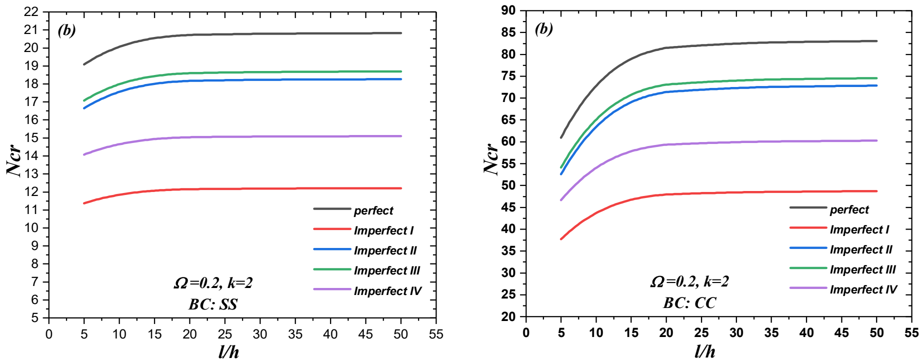

Fig. 4. The variation of buckling loads versus the side-to-thickness ratio l/h of perfect and imperfect beams ($k = 2$, $\Omega = 0.2$): a) *SS* boundary condition, b) *CC* boundary condition

5. Conclusions

This article presents a numerical study on the bending and buckling analysis of functionally graded beams using a simple integral shear deformation theory 2D and quasi-3D. The proposed beam has four types of porous distribution and was investigated under static bending and buckling with varied boundary conditions according to power law P-FGM distributions. This theory reduces the number of unknowns and governing equations while integrating the effects of thickness stretching into integral term. Analytical solutions for various boundary conditions for porous and perfect beams can be obtained by deriving the governing equations obtained from the static version of the principle of virtual work. Multiple validation examples are presented, and the current quasi-3D theory's numerical results accurately predict the bending and buckling responses of different FG porous beams. The theory satisfies the traction-free conditions on the top and bottom surfaces of the beam without using the shear correction factor. Closed-form solutions for static bending and buckling of beams with various boundary conditions are obtained.

References

[1] Zhang, N., Khan, T., Guo, H., Shi, S., Zhong, W., & Zhang, W. (2019). Functionally graded materials: An overview of stability, buckling, and free vibration analysis. *Adv. Mater. Sci. Eng.*, *2019*(5), 1-18.

[2] Dhuria, M., Grover, N., & Goyal, K. (2021). Influence of porosity distribution on static and buckling responses of porous functionally graded plates. *Structures*, 34, 1458-1474.

[3] Bouhadra, A., Menasria, A., & Rachedi, M.A. (2021). Boundary conditions effect for buckling analysis of porous functionally graded nanobeam. *Adv. Nano Res.*, *10*(4), 313-325.

[4] Reissner, E., & Stavsky, Y. (1961). Bending and stretching of certain types of heterogeneous aeolotropic elastic plates. *J. Appl. Mech.*, *28*(3), 402-408.

[5] Della Croce, L., & Venini, P. (2004). Finite elements for functionally graded Reissner-Mindlin plates. *Comp. Methods Appl. Mech. Eng.*, *193*(9-11), 705-725.

[6] Trabelsi, S., Frikha, A., Zghal, S., & Dammak, F. (2018). Thermal post-buckling analysis of functionally graded material structures using a modified FSDT. *Inter. J. Mech. Sci.*, *144*, 74-89.

[7] Zaitoun, M.W., Chikh, A., Tounsi, A., Al-Osta, M.A., Sharif, A., Al-Dulaijan, S.U., & Al-Zahrani, M.M. (2022). Influence of the visco-Pasternak foundation parameters on the buckling behavior of a sandwich functional graded ceramic-metal plate in a hygrothermal environment. *Thin-Walled Structures*, *170*, 108549.

[8] Slimani, R., Menasria, A., Ali Rachedi, M., Mourad, C., Refrafi, S., Nimer, A.A., Bouhadra, A., & Mamen, B. (2024). A novel quasi-3D refined HSDT for static bending analysis of porous functionally graded Plates. *J. Comp. Appl. Mech.*, *55*, 3, 519-537.

[9] Tounsi, A., Bouhadra, A., Bousahla, A.A., & Mahmoud, S. (2017). A new and simple HSDT for thermal stability analysis of FG sandwich plates. *Steel Comp. Struct., An International Journal*, *25*(2), 157-175.

[10] Messaoudi, A., Bouhadra, A., Menasria, A., Mamen, B., Boucham, B., Benguediab, M., Tounsi, A., & Al-Osta, M. (2023). Impact of the shear and thickness stretching effects on the free vibrations of advanced composite plates. *Mech. Comp. Mater.*, *59*(5), 1001-1018.

[11] Chitour, M., Bouhadra, A., Benguediab, S., Saoudi, A., Menasria, A., & Tounsi, A. (2022). Effect of phase contrast and geometrical parameters on bending behavior of sandwich beams with FG isotropic face sheets. *Journal of Nano- and Electronic Physics*, *14*(5).

[12] Tien, D.M., Thom, D.V., Minh, P.V., Tho, N.C., Doan, T.N., & Mai, D.N. (2024). The application of the nonlocal theory and various shear strain theories for bending and free vibration analysis of organic nanoplates. *Mechanics Based Design of Structures and Machines*, *52*(1), 588-610.

[13] Tuan, L.T., Dung, N.T., Van Thom, D., Van Minh, P., & Zenkour, A.M. (2021). Propagation of non-stationary kinematic disturbances from a spherical cavity in the pseudo-elastic cosserat medium. *Europ. Phys. J. Plus*, *136*, 1-16.

[14] Duong, V.Q., Tran, N.D., Luat, D.T., & Thom, D.V. (2022). Static analysis and boundary effect of FG-CNTRC cylindrical shells with various boundary conditions using quasi-3D shear and normal deformations theory. *Structures*, *44*, 828-850.

[15] Duc, D.H., Thom, D., & Phuc, P. (2022). Buckling analysis of variable thickness cracked nano-platesconsiderting the flexoelectric effect. *Trans. Commun. Sci. J.*, *73*(5), 470-485.

[16] Vu, V.T., Thom, D.V., & Tran, T.D. (2024). Identification of damage in steel beam by natural frequency using machine learning algorithms. *Proceedings of the Institution of Mechanical Engineers, Part C: Journal of Mechanical Engineering Science*, 09544062241255570.

[17] Ghazwani, M.H., Alnujaie, A., Youzera, H., Meftah, S.A., & Tounsi, A. (2024). Nonlinear forced vibration investigation of the sandwich porous FGM beams with viscoelastic core layer. *Acta Mech.*, *5*, 1-16.

[18] Patil, R., Joladarashi, S., & Kadoli, R. (2023). Effect of porosity and viscoelastic boundary conditions on FG sandwich beams in thermal environment: Buckling and vibration studies. *Structures*, *56*, 105001.

[19] Daikh, A.A., & Zenkour, A.M. (2019). Effect of porosity on the bending analysis of various functionally graded sandwich plates. *Mater. Res. Exp.*, *6*(6), 065703.

[20] Sayyad, A.S., & Ghugal, Y.M. (2018). Analytical solutions for bending, buckling, and vibration analyses of exponential functionally graded higher order beams. *Asian J. Civil Eng.*, *19*, 607-623.

[21] Timoshenko, S.P. (1921). On the correction for shear of the differential equation for transverse vibrations of prismatic bars. *Phil. Mag.*, *41*, 744-746.

[22] Reddy, J.N. (1984). A simple higher-order theory for laminated composite plates. *J. Appl. Mech.*, *51*(4), 745-752.

[23] Bernoulli, J. (1964). Curvatura laminae elasticae. *Acta Eruditorum Lipsiae*, *1694*(34), 262-276.

[24] Kahya, V., & Turan, M. (2017). Finite element model for vibration and buckling of functionally graded beams based on the first-order shear deformation theory. *Compos. Part B: Eng.*, *109*, 108-115.

[25] Nguyen, T.-K., Vo, T.P., & Thai, H.-T. (2013). Static and free vibration of axially loaded functionally graded beams based on the first-order shear deformation theory. *Compos. Part B: Eng.*, *55*, 147-157.